# Epitaxial Cubic Ce2O3 Films via Ce–CeO2 Interfacial Reaction

**ARTICLE** *in* JOURNAL OF PHYSICAL CHEMISTRY LETTERS · FEBRUARY 2013

Impact Factor: 7.46 · DOI: 10.1021/jz400187j

THE JOURNAL OF PHYSICAL CHEMISTRY Letters

Letter

pubs.acs.org/JPCL

# Epitaxial Cubic $Ce_2O_3$ Films via Ce–$CeO_2$ Interfacial Reaction

Vitalii Stetsovych,[†] Federico Pagliuca,[‡] Filip Dvořák,[†] Tomáš Duchoň,[†] Mykhailo Vorokhta,[†] Marie Aulická,[†] Jan Lachnitt,[†] Stefan Schernich,[§] Iva Matolínová,[†] Kateřina Veltruská,[†] Tomáš Skála,[†] Daniel Mazur,[†] Josef Mysliveček,*[,†] Jörg Libuda,[§] and Vladimír Matolín[†]

[†]Faculty of Mathematics and Physics, Charles University, V Holešovičkách 2, Praha 8, Czech Republic

[‡]Dipartimento di Scienze Fisiche, Informatiche e Matematiche, Università di Modena e Reggio Emilia and S3, Istituto Nanoscienze - CNR, Via G. Campi 213/a, 41125 Modena, Italy

[§]Lehrstuhl für Physikalische Chemie II and Erlangen Catalysis Resource Center, Friedrich-Alexander-Universität Erlangen-Nürnberg, Egerlandstrasse 3, 91058 Erlangen, Germany

**ABSTRACT:** Thin films of reduced ceria supported on metals are often applied as substrates in model studies of the chemical reactivity of ceria based catalysts. Of special interest are the properties of oxygen vacancies in ceria. However, thin films of ceria prepared by established methods become increasingly disordered as the concentration of vacancies increases. Here, we propose an alternative method for preparing ordered reduced ceria films based on the physical vapor deposition and interfacial reaction of Ce with $CeO_2$ films. The method yields bulk-truncated layers of cubic c-$Ce_2O_3$. Compared to $CeO_2$ these layers contain 25% of perfectly ordered vacancies in the surface and subsurface allowing well-defined measurements of the properties of ceria in the limit of extreme reduction. Experimentally, c-$Ce_2O_3$(111) layers are easily identified by a characteristic 4 × 4 surface reconstruction with respect to $CeO_2$(111). In addition, c-$Ce_2O_3$ layers represent an experimental realization of a normally unstable polymorph of $Ce_2O_3$. During interfacial reaction, c-$Ce_2O_3$ nucleates on the interface between $CeO_2$ buffer and Ce overlayer and is further stabilized most likely by the tetragonal distortion of the ceria layers on Cu. The characteristic kinetics of the metal–oxide interfacial reactions may represent a vehicle for making other metastable oxide structures experimentally available.

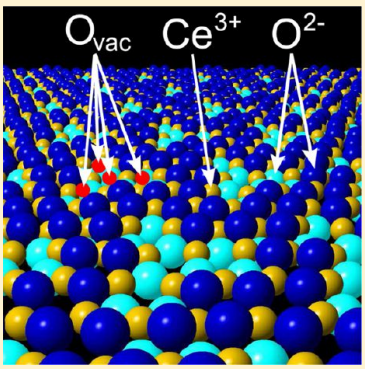


**SECTION:** Surfaces, Interfaces, Porous Materials, and Catalysis

An important property of ceria-based catalysts is the release and storage of oxygen in response to the changes of the reaction atmosphere.[1−3] The release and storage of oxygen is mediated by creation and annihilation of oxygen vacancies in ceria[4] and a continuous change of the ceria stoichiometry between two limiting cases, $CeO_2$ and $Ce_2O_3$.[5,6] It is primarily the oxygen vacancy distribution that determines the catalytic[7] and physical properties of ceria.[8] The importance of oxygen vacancies is reflected by a large body of experimental work, e.g., model studies of chemical reactivity over ordered thin films. Model studies on stoichiometric $CeO_2$(111) and on reduced $CeO_{2-x}$, $0 < x < 0.5$,[9−14] yielded information on reactivity and reaction mechanisms triggered by the presence or absence of oxygen vacancies.

Experimental strategies to prepare reduced ceria films include the deposition of metallic Ce at low pressure of oxygen,[9,12,14−16] the reduction of stoichiometric $CeO_2$ films by annealing in vacuum[17,18] or by adsorption and desorption of reducing species,[11,13,19] and the reduction by ion erosion.[10,20] The reduced films typically feature differences between surface and subsurface $Ce^{3+}$ concentrations[18,20] and an increase of disorder with increasing degree of reduction.[9,10,14,15] The latter often hampers the microscopic identification of surface and subsurface oxygen vacancies.[21,22] As a result of the complex dependency of the reducibility of the ceria layers on their morphology and preparation history, the analysis of the density and the distribution of the oxygen vacancies often relies on photoelectron spectroscopy.[23] The creation of an oxygen vacancy is accompanied by a release of two electrons from lattice $O^{2-}$ that accommodate in the bandgap of ceria in localized 4*f* states of two nearby $Ce^{4+}$ ions, changing their oxidation state to $Ce^{3+}$.[4] However, other sources of $Ce^{3+}$, e.g., undercoordinated Ce atoms at step edges[18,24] or ceria–metal interaction,[9,14,25,27] and variations of $Ce^{3+}$ depth profile must be considered carefully. As a result, quantification of surface and subsurface vacancies in reduced ceria layers is difficult, especially for higher degrees of reduction.

We propose an alternative method to prepare well-defined reduced ceria films. The method is based on physical vapor deposition of metallic Ce onto a stoichiometric $CeO_2$(111) film on Cu(111). We demonstrate that upon reactive interaction of the two components according to

$$3CeO_{2(s)} + Ce_{(s)} \xrightarrow{900\ K} 2Ce_2O_{3(s)} \quad (1)$$

**Received:** January 25, 2013
**Accepted:** February 27, 2013

   dx.doi.org/10.1021/jz400187j | *J. Phys. Chem. Lett.* 2013, 4, 866–871

it is possible to obtain highly ordered films of $Ce_2O_3$ on the Cu(111) substrate. The film stoichiometry is $Ce_2O_3$ as revealed by X-ray photoelectron spectroscopy (XPS), both at the surface and in the subsurface region (within the information depth of XPS, i.e., 3 nm). The surface structure of the films corresponds to a bulk-truncated cubic c-$Ce_2O_3$(111) (bixbyite). The bixbyite structure is obtained from the fluorite structure of $CeO_2$ by removing 25% O atoms and allowing a small relaxation.[4,6,26] The films exhibit perfectly ordered arrangement of surface and subsurface vacancies at a total concentration of 25% compared to $CeO_2$. The films are easily identified by low energy electron diffraction exhibiting a characteristic 4 × 4 reconstruction with respect to the $CeO_2$(111) surface. We expect that the ordered c-$Ce_2O_3$(111) films will be very suitable for model studies. They provide an atomically well-defined system for studies of reactivity of ceria-based catalysts at the limit of extreme reduction. Also they provide a very high density of surface vacancies for high-yield studies of their adsorption and reaction properties. Noteworthy, the structure of the films corresponds to the otherwise unstable cubic c-$Ce_2O_3$.[6] The stabilization of c-$Ce_2O_3$ may be related to the tetragonal distortion observed in c-$Ce_2O_3$ layers on Cu(111). The nucleation of c-$Ce_2O_3$ versus hexagonal a-$Ce_2O_3$ is traced back to the kinetics characteristic of the Ce-$CeO_2$ interfacial reaction rendering metal−oxide interfacial reactions as an interesting tool for experimental realization of metastable oxide structures.

The morphology of a ceria film undergoing reaction 1 is shown in Figure 1. As a starting point, an ordered $CeO_2$ buffer layer—a continuous layer of $CeO_2$(111) on Cu(111)—was prepared according to Dvořák et al.[18] The sample temperature used for preparation of the ceria buffer was 520 K, and the film thickness was 4 ML. Here, 1 ML of ceria is defined as an O−Ce−O trilayer, corresponding to the vertical stacking of O and Ce layers in $CeO_2$(111) and/or c-$Ce_2O_3$(111), with Ce atom density of $7.9 \times 10^{14}$ $cm^{-2}$. Figure 1a shows that the ordered $CeO_2$ buffer consists of stacks of 1 ML-high $CeO_2$(111) islands covering the whole surface. The characteristic terrace width using the above preparation conditions is 10 nm.[18] Upon deposition of metallic Ce, the surface becomes disordered (see Figure 1b). A much improved ordering, however, is re-established after annealing of the buffer with Ce deposit to 900 K for 30 min in vacuum. The resulting morphology is shown in Figure 1(c). We obtain a flat film with an average terrace width of 30 nm. Nearly all step edges are found to be aligned in high-symmetry directions. On the complete surface, STM reveals a characteristic surface reconstruction shown in the inset of Figure 1c. The unit cell of the reconstruction is 1.5 nm, i.e., about 4 times the size of the unit cell of the unreconstructed $CeO_2$(111)1 × 1 surface. The 4 × 4 reconstruction of ceria after reaction 1 is confirmed by low energy electron diffraction (LEED) in Figure 2a. For comparison, a LEED pattern of the ordered $CeO_2$ buffer layer is shown in Figure 2b. In addition to the qualitative 4 × 4 reconstruction, LEED reveals a slight expansion of the in-plane lattice constant after reaction 1.

The characteristic 4 × 4 reconstruction observed after reaction 1 allows a straightforward preparation and characterization of the reduced film even if no STM is available. We have repeated the experiments in different experimental chambers finding the same LEED pattern. In an XPS system, the stoichiometry of the films was analyzed before and after reaction. We measured the Ce 3d and O 1s levels (Figure 3)

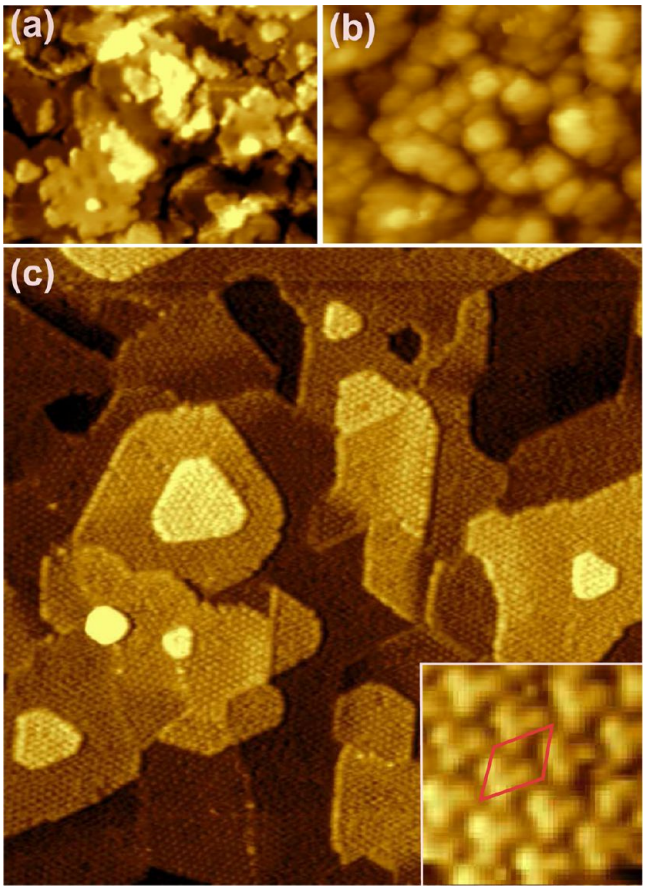


**Figure 1.** Scanning tunneling microscopy images of the reaction between Ce and the $CeO_2$ buffer layer: (a) ordered $CeO_2$ buffer, (b) disordered surface upon Ce deposition, (c) ordered layer upon annealing in vacuum at 900 K. Inset: high-resolution image and surface unit cell (red rhombus) of the reacted layer. Images a−c are to scale. Image width (a,b) 60 nm, (c) 120 nm, (inset) 6 × 6 $nm^2$.

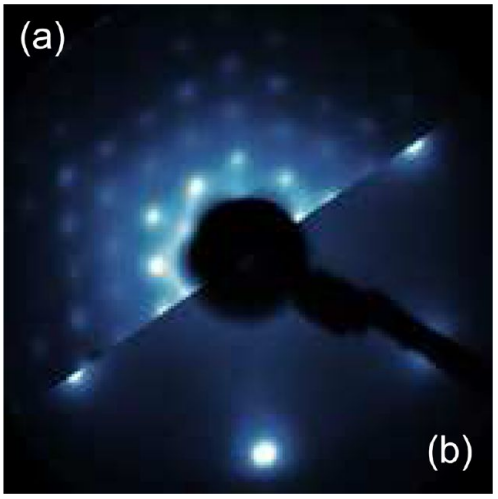


**Figure 2.** LEED image of the reaction between Ce and $CeO_2$ buffer layer: (a) reacted layer, (b) starting $CeO_2$ buffer. Electron energy 55 eV.

and performed resonant photoelectron spectroscopy (RPES, Figure 4). The Ce 3d spectra of the ordered $CeO_2$(111) buffer film (Figure 3, thin lines) and the film after reaction with Ce (Figure 3, thick lines) reveal pure $Ce^{4+}$ spectrum (as in $CeO_2$)


dx.doi.org/10.1021/jz400187j | J. Phys. Chem. Lett. 2013, 4, 866−871

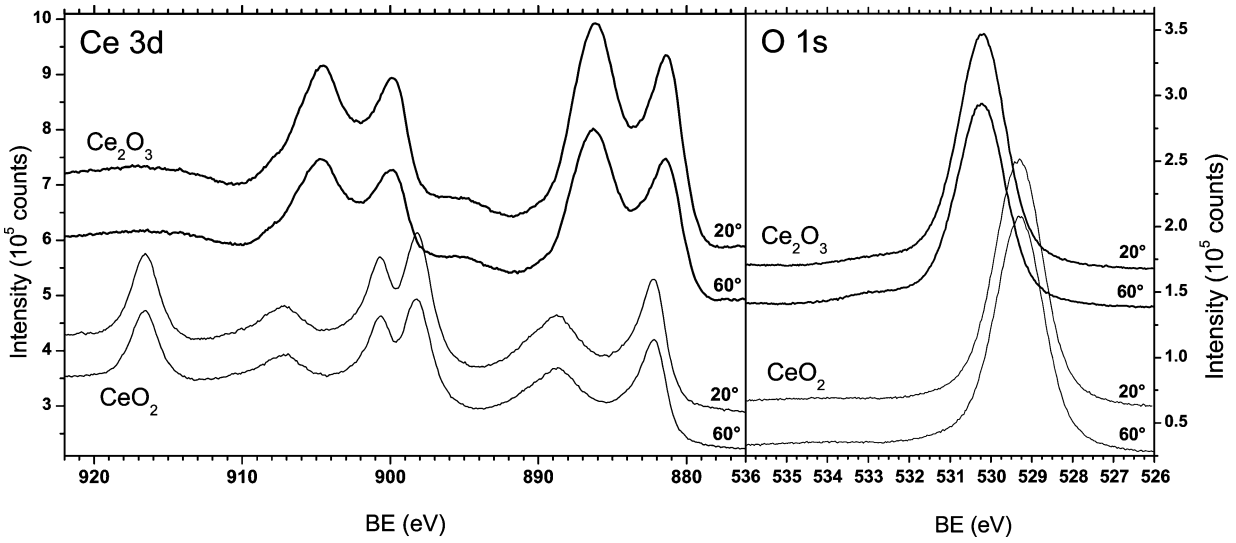


**Figure 3.** Photoelectron spectroscopy of cerium (Ce 3d) and lattice oxygen ions (O 1s) after the reaction between Ce and $CeO_2$ buffer layer (thick lines) and the starting $CeO_2$ buffer (thin lines). Measurements are performed for 20° and 60° off-normal emission. Amplitudes as measured, curves offset for better visibility.

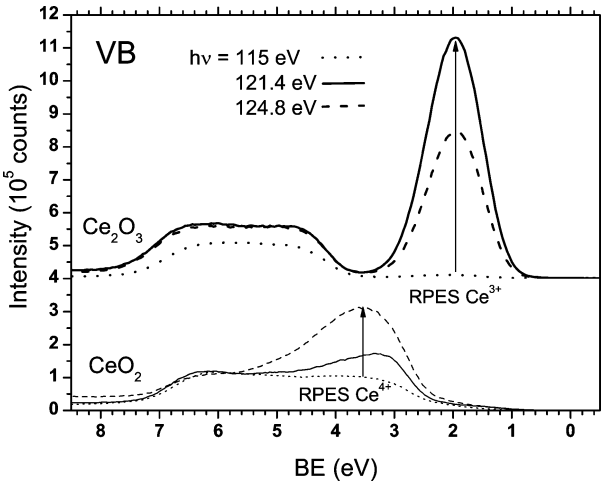


**Figure 4.** Resonant photoelectron spectroscopy after the reaction between Ce and $CeO_2$ buffer layer (thick lines) and the starting $CeO_2$ buffer (thin lines). Photon energy is 115 eV for off-resonance (dotted line), 121.4 eV for $Ce^{3+}$ resonance (dashed line), and 124.8 eV for $Ce^{4+}$ resonance (solid line).

and pure $Ce^{3+}$ spectrum (as in $Ce_2O_3$), respectively.[23,25] The deviation from ideal $Ce_2O_3$ and $CeO_2$ stoichiometries are below the detection limit of the standard fitting procedures,[14,25,28] which is about 2% $Ce^{4+}$ in $Ce^{3+}$ and vice versa. Transformation of $CeO_2$ into $Ce_2O_3$ is accompanied by a shift of O 1s level from 529.25 eV to higher binding energy 530.20 eV (Figure 3).[23] We have also used the extremely sensitive RPES to determine the $Ce^{3+}$ and $Ce^{4+}$ concentrations.[29,30] The $Ce^{3+}$ resonance of the $Ce_2O_3$ layer appears at 1.95 eV shifted to a higher energy with respect to the $Ce^{3+}$ resonance of partially reduced $CeO_{2-x}$ layers (1.5 eV).[10] Analysis of the RPES data reveals no $Ce^{3+}$ contribution in the $CeO_2$ buffer layer (Figure 4, thin lines) and no $Ce^{4+}$ contribution (at 3.56 eV) in the $Ce_2O_3$ layer after reaction 1 (Figure 4, thick lines). From the attenuation of the XPS signal of the substrate (Cu $2p_{3/2}$) the thickness of the ordered $CeO_2$ buffer was determined to be 2.8 nm. The thickness of the $Ce_2O_3$ layer after reaction was calculated to be 3.9 nm. The increase in layer thickness occurs upon Ce deposition and transformation of $CeO_2$ into $Ce_2O_3$ according to reaction 1. Measuring the XPS at different emission angles 20° and 60° off normal reveals no change in the stoichiometry of the layers with the emission angle, which, together with the results from RPES, indicates that both before and after reaction the films are bulk-terminated $CeO_2$ and $Ce_2O_3$, respectively. Both $CeO_2$ buffer and $Ce_2O_3$ layer were determined by ISS to be oxygen terminated. Decreasing the angle of the incident ion beam relative to the surface plane, the Ce signal was observed to disappear at 15°, while the O signal was still clearly visible at 10° with respect to the surface plane.[15]

An important consequence of the reduction and oxidation of ceria are the changes of the lattice constant, which are proportional to the concentration of oxygen vacancies.[1−3,8] Thus, the reduction of ceria may be viewed of as an isostructural transition between cubic $CeO_2$ and cubic $CeO_{2-x}$ with the Ce sublattice in $CeO_{2-x}$ attaining its fcc structure and increasing its lattice constant as the oxygen vacancies are created in the cubic O sublattice.[4] In our experiment, the changes of the in-plane lattice constant were followed by LEED and summarized in Table 1. The in-plane lattice constant we are referring to is $1/\sqrt{2}$ of the bulk lattice constant of the fluorite $CeO_2$ or $1/2\sqrt{2}$ of the bulk lattice constant of the bixbyite c-$Ce_2O_3$. The $CeO_2$ buffer (Figure 1a) exhibits a contracted in-plane lattice constant of 3.71 Å. Such contraction is typical for metal-supported ceria films.[18,21,28,31]

**Table 1. Changes of Thickness, Stoichiometry and In-Plane Lattice Constant of the Ceria Films upon the Reaction between Ce and $CeO_2$ and Subsequent Oxidation**

| | $CeO_2$ buffer | upon reaction with Ce | upon oxidation |
|---|---|---|---|
| thickness (ML) | 4 | 6 | 6 |
| stoichiometry | $CeO_2$ | $Ce_2O_3$ | $CeO_2$ |
| in-plane lattice constant (Å) | 3.71 | 3.84 | 3.74 |
| in-plane lattice constant change | | +3.5% | −2.6% |


dx.doi.org/10.1021/jz400187j | J. Phys. Chem. Lett. 2013, 4, 866−871

After the reaction 1 (Figure 1c), the in-plane lattice constant increases to 3.84 Å (+3.5%). However, the reaction 1 is accompanied by an increase of the thickness of the ceria layer. In order to exclude the effect of possible thickness-dependencies of the in-plane lattice constant[31] we performed oxidation of the $Ce_2O_3$ layer after reaction 1 by exposure to 10 000 L $O_2$ at a sample temperature of 900 K. This procedure fully restores the $CeO_2$ stoichiometry and the 1 × 1 termination of the layer. An almost complete oxidation of the $Ce_2O_3$ layer is, however, obtained much earlier, at about 200 L $O_2$.[26] Upon oxidation, the in-plane lattice constant decreases to 3.74 Å (−2.6%). This change can be regarded as corresponding solely to the transition from $Ce_2O_3$ to $CeO_2$ in a 6 ML thick ceria film on Cu(111). The fact that the change of the in-plane lattice constant of the thin film $Ce_2O_3$ and $CeO_2$ (−2.6%, 3.84 Å, 3.74 Å) are smaller than those of the corresponding bulk system c-$Ce_2O_3$ and $CeO_2$ (−3%, 3.95 Å, 3.83 Å),[6] are attributed to the finite size effect in the ceria layer that becomes effective on the copper substrate.[32] Still, the change distinctly confirms the observed bulk oxidation and reduction in the ceria layers.

The structure of the $Ce_2O_3$ upon the isostructural change from $CeO_2$ was theoretically predicted to be cubic bixbyite c-$Ce_2O_3$.[4] In bulk experiments, however, cubic $CeO_{2-x}$ is reported for $x$ up to 0.32.[33] For $x$ = 0.5, the stable form is the hexagonal a-$Ce_2O_3$.[6,34−36] Also, $Ce_2O_3$ thin films are generally suggested to adopt hexagonal a-$Ce_2O_3$ structure, based on the combination of photoelectron spectroscopy data and the hexagonal 1 × 1 LEED pattern that is typically observed.[14,17,37,38] A notable exception is the c-$Ce_2O_3$ layer on Si proposed by Flege et al.[39] However, the comparability of this system is limited by the fact that Si interdiffuses into ceria and inhibits the oxygen storage capacity.[40]

It should also be noted that the (0001) surface of a-$Ce_2O_3$ is not charge neutral, and its existence as a bulk layer termination requires some form of charge compensation, e.g., by additional oxygen vacancies.[17] In c-$Ce_2O_3$(111), on the other hand, the charge neutrality is fulfilled. The interpretation of high-resolution ISS of highly reduced ceria films also favors the cubic bixbyite structure.[15] In our thin film system, the preferential assignment to c-$Ce_2O_3$(111) rather than to a-$Ce_2O_3$(0001) primarily originates from the interpretation of the LEED pattern. The 4 × 4 reconstruction relative to $CeO_2$(111) rules out the a-$Ce_2O_3$(0001) structure. For comparison with the bixbyite termination, we plot a top view of the fluorite $CeO_2$(111) and the bixbyite c-$Ce_2O_3$(111) bulk terminations in Figure 5a,b. The structure of bixbyite c-$Ce_2O_3$(111) is adopted from the data in the Inorganic Crystal Structure Database, ICSD #96202.[41] In perfect agreement with the LEED observation, the surface unit cell of this c-$Ce_2O_3$(111) plane is 4 × 4 times larger than the surface unit cell of $CeO_2$(111). In c-$Ce_2O_3$(111) (Figure 5b) we can outline the structural motif generated by the surface oxygen vacancies (black line). The position and orientation of the obtained 3-fold motif inside the unit cell perfectly corresponds to the STM image of the $Ce_2O_3$ layer (inset of Figure 1c).

It may seem misleading in this place to speak of oxygen vacancies in a stoichiometric c-$Ce_2O_3$. However, in this contribution, the term "oxygen vacancies" is always used to describe missing O atoms in the flourite structure of $CeO_{2-x}$. These can be identified, due to the similarity of the crystal structures, even in the bixbyite c-$Ce_2O_3$. Indeed, the locations of (apparently) missing surface O atoms outlined in Figure 5b locally reveal much the same arrangement of $O^{2-}$ and exposed

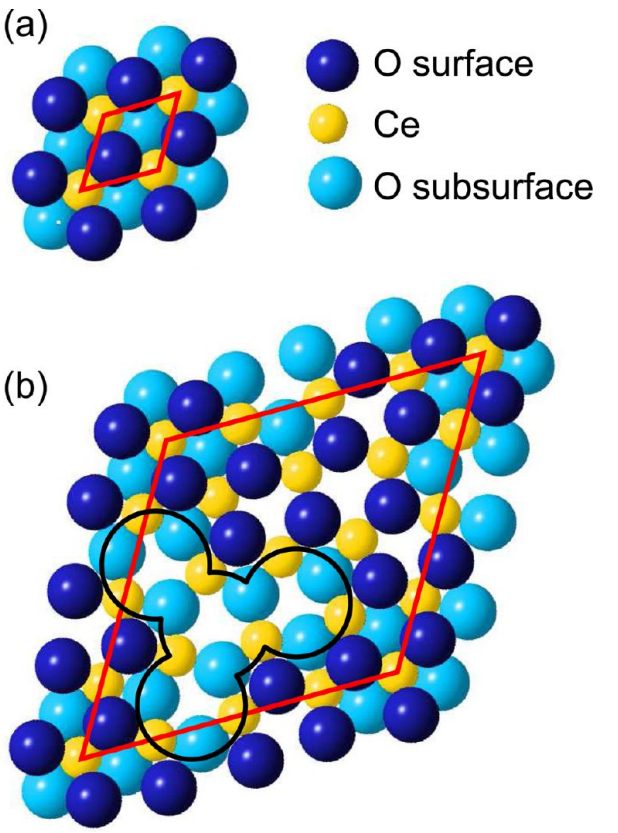


**Figure 5.** Schematic top view of a bulk-truncated $CeO_2$(111) (a) and cubic $Ce_2O_3$(111) (b). Surface unit cells are marked red in both a and b. In b, the structural motif of surface oxygen vacancies is outlined black.

underlying $Ce^{3+}$ atoms as do the surface O vacancies on thermally reduced surfaces of $CeO_{2-x}$.[22] Also, the RPES reveals that the occupied Ce 4*f* electron state in the bandgap as observed on partially reduced $CeO_{2-x}$ remains occupied also in our c-$Ce_2O_3$ layers (Figure 4). Thus, in terms of the atom arrangement and the electron structure, the (111) surface of the bixbyite c-$Ce_2O_3$ can be considered as a limiting case of the reduced $CeO_{2-x}$(111) surface maximizing its chemical reactivity through maximizing the available surface $Ce^{3+}$ atoms. Other favorable properties of reduced ceria may, however, be vanishing in the limit of complete reduction to $Ce_2O_3$. This concerns mainly the electrical conductivity of $CeO_{2-x}$ that is mediated by the concerted activated motion of the electrons localized in Ce 4*f* states and the oxygen vacancies.[8]

The stabilization of the c-$Ce_2O_3$ structure in preference of the a-$Ce_2O_3$ in the thin film may be due to the interaction with the Cu(111) substrate. Copper substrate allows a contraction of the in-plane lattice constant of the ceria layer[32] and, as a consequence, a tetragonal distortion of the ceria layer that can stabilize the c-$Ce_2O_3$. The in-plane contraction of ceria on Cu(111) amounts to approximately 3%, a larger value than, e.g., on Pt(111), where 1% contraction is observed.[21,28] The interfacial reaction between Ce and $CeO_2$, however, brings about a drastic change in the kinetics of formation of reduced ceria as well.[42] With all previously proposed methods to prepare thin films of reduced ceria, either $O_2$ is removed from the surface of $CeO_2$ or $O_2$ is adsorbed on Ce metal, ultimately leading to nucleation of the a-$Ce_2O_3$ phase on the surface. In contrast, the present preparation method involves only bulk


dx.doi.org/10.1021/jz400187j | J. Phys. Chem. Lett. 2013, 4, 866−871

diffusion of oxygen ions between $CeO_2$ buffer layer and Ce overlayer. This very different formation mechanism involving an interfacial reaction at the Ce−ceria interface obviously favors nucleation of c-$Ce_2O_3$. Comparing, e.g., to reduction of the $CeO_2$(111) surface by $Ar^+$ sputtering and thermal annealing in vacuum, where temperatures exceeding 1150 K are needed to create a few percent surface vacancies,[22] the distinct kinetics of the interfacial reaction between Ce and $CeO_2$ (1) bypasses this rate-limiting step, arriving at a complete surface and bulk reduction of the layer at a considerably lower temperature of 900 K.

To conclude, we have demonstrated that interfacial reaction of a stoichiometric $CeO_2$ thin film on Cu(111) with deposited metallic Ce yields a highly ordered layer of cubic bixbyite c-$Ce_2O_3$(111). The surface structure of the layer corresponds to bulk-terminated c-$Ce_2O_3$(111). It contains ordered vacancy clusters, each consisting of four oxygen vacancies. With these vacancy clusters both in the surface and subsurface O layers, 25% of vacancies are generated in total compared to $CeO_2$. The surface exhibits a very characteristic and sharp 4 × 4 LEED pattern relative to $CeO_2$(111), allowing easy experimental identification. We suggest that the c-$Ce_2O_3$(111) film is a unique model experimental system for highly reduced ceria surfaces. It provides an atomically well-defined surface exposing exclusively $Ce^{3+}$ ions and a high density of oxygen vacancies with a precisely defined environment. In future work, we will explore the interfacial reaction of deposited Ce metal with ceria to prepare ordered reduced ceria films with lower vacancy concentrations. The c-$Ce_2O_3$(111) film also represents an experimental realization of a normally unstable cubic c-$Ce_2O_3$. The stabilization of cubic c-$Ce_2O_3$ appears most likely due to a tetragonal distortion of c-$Ce_2O_3$ thin film on Cu surfaces. The nucleation of cubic c-$Ce_2O_3$, on the other hand, can be traced back to the distinct kinetics of the interfacial reaction between Ce and $CeO_2$. This allows us to suggest interfacial reactions between metals and oxides as viable tools for experimental realization of metastable oxide structures.

## EXPERIMENTAL METHODS

The experiments were performed in two ultrahigh vacuum systems in Prague, and at the Material Science Beamline at Synchrotron Elettra (Trieste, Italy).[10,13,16,18,19,25,29] All systems have a base pressure of 1 × $10^{-8}$ Pa, feature the required sample cleaning and preparation facilities, and LEED optics. For surface characterization, one or more of the following techniques were available in each system: XPS using laboratory sources or synchrotron radiation, RPES, ion scattering spectroscopy (ISS), and/or scanning tunneling microscopy (STM). Cu(111) single crystals (MaTecK) were cleaned by $Ar^+$ bombardment and annealing in vacuum. Ce (Goodfellow) was evaporated from tantalum or molybdenum crucibles heated by electron bombardment in the background atmosphere of 5 × $10^{-5}$ Pa of $O_2$ (Linde, 5.0) for the growth of $CeO_2$(111) buffers or in vacuum for the deposition of metallic Ce. The thickness of the ceria films was determined from the attenuation of Cu $2p_{3/2}$ in XPS or by a quartz crystal microbalance. Photoelectron spectroscopy of the Ce 3d, O 1s and Cu $2p_{3/2}$ core levels was performed with X-ray radiation of 1486.6 eV (Al k$\alpha$), and RPES of the ceria valence band was performed with synchrotron radiation in the range 115−125 eV. Ion scattering was performed with $He^+$ ions with energy 1500 eV. STM of ceria layers was performed with chemically etched tungsten tips annealed in vacuum. STM images were obtained by tunneling into the unoccupied states of the sample. All measurements were performed at room temperature. Surface reconstruction, surface termination, and stoichiometry of the layers measured by LEED, ISS, and XPS remained unaltered also at an elevated sample temperature of 570 K, which allows us to exclude the influence of unintentional adsorption during our experiments.

## AUTHOR INFORMATION

### Corresponding Author

*E-mail: josef.myslivecek@mff.cuni.cz.

### Notes

The authors declare no competing financial interest.

## ACKNOWLEDGMENTS

This work was supported by the Grant Agency of the Czech Republic (GAČR 204/11/1183) and by the Ministry of Education of the Czech Republic (LG12003). V.S. and F.D. acknowledge the support of the Grant Agency of the Charles University (GAUK 339311, GAUK 610112). We also acknowledge the support by the EU via the FP7 NMP Project No. 310191 "chipCAT" and via the COST Action CM1104 (Reducible Oxides, Structure and Function). J.L. (Erlangen) acknowledges additional support by the DAAD (German Academic Exchange Service). We gratefully acknowledge helpful discussions with Lucie Szabová, Karel Mašek, and Jan Beran. We would also like to thank Radomír Kužel for the discussion of ICSD data.

## REFERENCES

(1) Wang, X.; Rodriguez, J. A.; Hanson, J. C.; Gamarra, D.; Martínez-Arias, A.; Fernández-García, M. In Situ Studies of the Active Sites for the Water Gas Shift Reaction over Cu-$CeO_2$ Catalysts: Complex Interaction between Metallic Copper and Oxygen Vacancies of Ceria. *J. Phys. Chem. B* **2006**, *110*, 428−434.

(2) Xu, W.; Si, R.; Senanayake, S. D.; Llorca, J.; Idriss, H.; Stacchiola, D.; Hanson, J. C.; Rodriguez, J. A. In Situ Studies of $CeO_2$-supported Pt, Ru, and Pt−Ru Alloy Catalysts for the Water−Gas Shift Reaction: Active Phases and Reaction Intermediates. *J. Catal.* **2012**, *291*, 117−126.

(3) Trovarelli, A. *Catalysis by Ceria and Related Materials*; Imperial College Press: London, 2002.

(4) Skorodumova, N. V.; Simak, S. I.; Lundqvist, B. I.; Abrikosov, I. A.; Johansson, B. Quantum Origin of the Oxygen Storage Capability of Ceria. *Phys. Rev. Lett.* **2002**, *89*, 166601.

(5) Fabris, S.; de Gironcoli, S.; Baroni, S.; Vicario, G.; Balducci, G. Taming Multiple Valency with Density Functionals: A Case Study of Defective Ceria. *Phys. Rev. B* **2005**, *71*, 041102(R).

(6) Da Silva, J. L. F. Stability of the $Ce_2O_3$ Phases: A DFT+U Investigation. *Phys. Rev. B* **2007**, *76*, 193108.

(7) Lawrence, N. L.; Brewer, J. R.; Wang, L.; Wu, T.-S.; Wells-Kingsbury, J.; Ihrig, M. M.; Wang, G.; Soo, Y.-L.; Mei, W.-N.; Cheung, C. L. Defect Engineering in Cubic Cerium Oxide Nanostructures for Catalytic Oxidation. *Nano Lett.* **2011**, *11*, 2666−2671.

(8) Mogensen, M.; Sammes, N. M.; Tompsett, G. A. Physical, Chemical, and Electrochemical Properties of Pure and Doped Ceria. *Solid State Ionics* **2000**, *63*, 63−94.

(9) Zhou, Y.; Perket, J. M.; Zhou, J. Growth of Pt Nanoparticles on Reducible $CeO_2$(111) Thin Films: Effect of Nanostructures and Redox Properties of Ceria. *J. Phys. Chem. C* **2010**, *114*, 11853−11860.

(10) Matolín, V.; Matolínová, I.; Dvořák, F.; Johánek, V.; Mysliveček, J.; Prince, K. C.; Skála, T.; Stetsovych, O.; Tsud, N.; Václavů, M.; Šmíd, B. Water Interaction with $CeO_2$(111)/Cu(111) Model Catalyst Surface. *Cat. Today* **2012**, *181*, 124−132.

(11) Senanayake, S. D.; Stacchiola, D.; Evans, J.; Estrella, M.; Barrio, L.; Pérez, M.; Hrbek, J.; Rodriguez, J. A. Probing the Reaction

Intermediates for the Water-Gas Shift over Inverse $CeO_x$/Au(111) Catalysts. *J. Catal.* **2010**, *271*, 392−400.
(12) Gordon, W. O.; Xu, Y.; Mullins, D. R.; Overbury, S. H. Temperature Evolution of Structure and Bonding of Formic Acid and Formate on Fully Oxidized and Highly Reduced $CeO_2$(111). *Phys. Chem. Chem. Phys.* **2009**, *11*, 11171−11183.
(13) Lykhach, Y.; Johánek, V.; Aleksandrov, H. A.; Kozlov, S. M.; Happel, M.; Skála, T.; Petkov, P. S.; Tsud, N.; Vayssilov, G. N.; Prince, K. C.; Neyman, K. M.; Matolín, V.; Libuda, J. Water Chemistry on Model Ceria and Pt/Ceria Catalysts. *J. Phys. Chem. C* **2012**, *116*, 12103−12113.
(14) Wilson, E. L.; Chen, Q.; Brown, W. A.; Thornton, G. CO Adsorption on the Model Catalyst Pd/$CeO_{2-x}$(111)/Rh(111). *J. Phys. Chem. C* **2007**, *111*, 14215−14222.
(15) Mullins, D. R.; Radulovic, P. V.; Overbury, S. H. Ordered Cerium Oxide Thin Films Grown on Ru(0001) and Ni(111). *Surf. Sci.* **1999**, *429*, 186−198.
(16) Matolín, V.; Libra, J.; Matolínová, I.; Nehasil, V.; Sedláček, L.; Šutara, F. Growth of Ultra-Thin Cerium Oxide Layers on Cu(111). *Appl. Surf. Sci.* **2007**, *254*, 153−155.
(17) Berner, U.; Schierbaum, K.-D. Cerium Oxides and Cerium−Platinum Surface Alloys on Pt(111) Single-Crystal Surfaces Studied by Scanning Tunneling Microscopy. *Phys. Rev. B* **2002**, *65*, 235404.
(18) Dvořák, F.; Stetsovych, O.; Steger, M.; Cherradi, E.; Matolínová, I.; Tsud, N.; Škoda, M.; Skála, T.; Mysliveček, J.; Matolín, V. Adjusting Morphology and Surface Reduction of $CeO_2$(111) Thin Films on Cu(111). *J. Phys. Chem. C* **2011**, *115*, 7496−7503.
(19) Matolín, V.; Libra, J.; Škoda, M.; Tsud, N.; Prince, K. C.; Skála, T. Methanol Adsorption on a $CeO_2$(111)/Cu(111) Thin Film Model Catalyst. *Surf. Sci.* **2009**, *603*, 1087−1092.
(20) Wang, G. D.; Kong, D. D.; Pan, Y. H.; Pan, H. B.; Zhu, J. F. Low Energy Ar-Ion Bombardment Effects on the $CeO_2$ Surface. *Appl. Surf. Sci.* **2012**, *258*, 2057−2061.
(21) Grinter, D. C.; Ithnin, R.; Pang, C. L.; Thornton, G. Defect Structure of Ultrathin Ceria Films on Pt(111): Atomic Views from Scanning Tunnelling Microscopy. *J. Phys. Chem. C* **2010**, *114*, 17036−17041.
(22) Esch, F.; Fabris, S.; Zhou, L.; Montini, T.; Africh, C.; Fornasiero, P.; Comelli, G.; Rosei, R. Electron Localization Determines Defect Formation on Ceria Substrates. *Science* **2005**, *309*, 752−755.
(23) Mullins, D. R.; Overbury, S. H.; Huntley, D. R. Electron Spectroscopy of Single Crystal and Polycrystalline Cerium Oxide Surfaces. *Surf. Sci.* **1998**, *409*, 307−319.
(24) Lu, J.-L.; Gao, H.-J.; Shaikhutdinov, S.; Freund, H.-J. Morphology and Defect Structure of the $CeO_2$(111) Films Grown on Ru(0001) as Studied by Scanning Tunneling Microscopy. *Surf. Sci.* **2006**, *600*, 5004−5010.
(25) Skála, T.; Šutara, F.; Prince, K. C.; Matolín, V. Cerium Oxide Stoichiometry Alteration via Sn Deposition: Influence of Temperature. *J. Electron Spectrosc. Relat. Phenom.* **2009**, *169*, 20.
(26) Creaser, D. A.; Harrison, P. G.; Morris, M. A.; Wolfindale, B. A. X-ray Photoelectron Spectroscopic Study of the Oxidation and Reduction of a Cerium(III) Oxide/Cerium Foil. *Catal. Lett.* **1994**, *23*, 13−24.
(27) Castellarin-Cudia, C.; Surnev, S.; Schneider, G.; Podlucky, R.; Ramsey, M. G.; Netzer, F. P. Strain-Induced Formation of Arrays of Catalytically Active Sites at the Metal−Oxide Interface. *Surf. Sci.* **2004**, *554*, L120−L126.
(28) Luches, P.; Pagliuca, F.; Valeri, S. Morphology, Stoichiometry, and Interface Structure of $CeO_2$ Ultrathin Films on Pt(111). *J. Phys. Chem. C* **2011**, *115*, 10718−10726.
(29) Škoda, M.; Cabala, M.; Matolínová, I.; Prince, K. C.; Skála, T.; Šutara, F.; Veltruská, K.; Matolín, V. Interaction of Au with $CeO_2$(111): A Photoemission Study. *J. Chem. Phys.* **2009**, *130*, 034703.
(30) Matsumoto, M.; Soda, K.; Ichikawa, K.; Tanaka, S.; Taguchi, Y.; Jouda, K.; Aita, O.; Tezuka, Y.; Shin, S. Resonant Photoemission Study of $CeO_2$. *Phys. Rev. B* **1994**, *50*, 11340−11346.
(31) Mašek, K.; Beran, J.; Matolín, V. RHEED Study of the Growth of Cerium Oxide on Cu(111). *Appl. Surf. Sci.* **2012**, *259*, 34−38.
(32) Stetsovych, O.; Dvořák, F.; Szabová, L.; Fabris, S.; Mysliveček, J.; Matolín, V. Nanometer-Range Strain Distribution in Layered Incommensurate Systems. *Phys. Rev. Lett.* **2012**, *109*, 266102.
(33) Kümmerle, J. A.; Heger, G. J. The Structures of C-$Ce_2O_{3+\delta}$, $Ce_7O_{12}$, and $Ce_{11}O_{20}$. *J. Solid State Chem.* **1999**, *147*, 485−500.
(34) Pinto, H.; Mintz, M. H.; Melamud, M.; Shaked, H. Neutron Diffraction Study of $Ce_2O_3$. *Phys. Lett.* **1982**, *88A*, 81−83.
(35) Bäringhausen, H.; Schiller, G. The Crystal Structure of A-$Ce_2O_3$. *J. Less-Common Met.* **1985**, *110*, 385−390.
(36) Huntelaar, M. E.; Booij, A. S.; Cordfunke, E. H. P.; van der Laan, R. R. The Thermodynamic Properties of $Ce_2O_3$(s) from $T \rightarrow 0$ to 1500 K. *J. Chem. Thermodynamics* **2000**, *32*, 465−482.
(37) Vescovo, E.; Carbone, C. Oxidation of Epitaxial Ce Films. *Phys. Rev. B* **1996**, *53*, 4142−4147.
(38) Xiao, W.; Guo, Q.; Wang, E. G. Transformation of $CeO_2$(111) to $Ce_2O_3$(0001) Films. *Chem. Phys. Lett.* **2003**, *368*, 527−531.
(39) Flege, J. I.; Kaemena, B.; Gevers, S.; Bertram, F.; Wilkens, T.; Bruns, D.; Bätjer, J.; Schmidt, T.; Wollschläger, J.; Falta, J. Silicate-Free Growth of High-Quality Ultrathin Cerium Oxide Films on Si(111). *Phys. Rev. B* **2011**, *84*, 235418.
(40) Pagliuca, F.; Luches, P.; Valeri, S. Interfacial Interaction Between Cerium Oxide and Silicon Surfaces. *Surf. Sci.* **2013**, *607*, 164−169.
(41) Hirosaki, N.; Ogata, S.; Kocer, C. Ab Initio Calculation of the Crystal Structure of the Lanthanide $Ln_2O_3$ Sesquioxides. *J. Alloys Compd.* **2003**, *351*, 31−34.
(42) Mayer, J. T.; Diebold, U.; Madey, T. E.; Garfunkel, E. Titanium and Reduced Titania Overlayers on Titanium Dioxide(110). *J. Electron Spectrosc. Relat. Phenom.* **1995**, *73*, 1−11.